Optimized single-step (OSS) chemistry for auto-ignition of heterogeneous mixtures

Luis Carbajal-Carrasco, Zakaria Bouali, Arnaud Mura

Optimized single-step (OSS) chemistry for auto-ignition of heterogeneous mixtures

Luis A. Carbajal-Carrasco[a], Zakaria Bouali[a], Arnaud Mura[a,*]

[a]*PPRIME UPR3346 CNRS, ENSMA and University of Poitiers, 1 Avenue Clément Ader, 86961 Futuroscope Chasseneuil, France*

Abstract

With the objective of recovering the values of ignition delays of reactive heterogeneous mixtures a single-step chemistry model has been developed. The corresponding model extends a recent optimization procedure introduced to describe flame propagation in heterogeneous media featuring composition variations (equivalence ratio and temperature) in the fresh reactants or containing residual burned gases (RBG). It is based on the use of an optimized virtual species and a tabulation of the pre-exponential coefficient of an Arrhenius law. The main results of high activation energy asymptotics (AEA) are first recalled to put in evidence the key parameters and the dependence of the ignition delay on the corresponding quantities. The optimization procedure is then applied to these parameters, namely, the pre-exponential factor K and the activation energy E_a of the associated single-step Arrhenius law. An efficient tabulation method benefiting from both rapid access and low storage is proposed for the composition variable (the mixture fraction, in the present case). Finally, the restitution of both ignition and propagation features is ensured through the consideration of the cross-over temperature. The performance of the resulting model is then assessed through comparisons with data obtained from detailed chemistry computations used as reference in several conditions of increasing complexity.

Keywords: single-step chemistry, auto-ignition, ignition delay, premixed combustion, turbulent flames

*Corresponding author.
Email address: arnaud.mura@ensma.fr (Arnaud Mura)

1. General Introduction

In numerical simulations of turbulent combustion, the model used to represent the chemical mechanism plays a crucial role [1]. Even though major technical breakthroughs have been reached in high-performance computing (HPC), the use of detailed chemistry [2, 3] still remains quite computationally demanding. Therefore, several strategies have been proposed to circumvent this limitation. Early studies applied sensitivity analysis on detailed chemistry schemes to obtain skeletal mechanisms [4, 5] which consider only a reduced set of chemical reactions and species based on their predominance. More cost-efficient reduced chemical schemes [6–10] can be achieved by considering the quasi-steady state approximation (QSSA) of some chemical species. This method significantly decreases the computational time when compared to skeletal or complex schemes. Nevertheless, depending on the domain size, the computational cost of the required species may still reveal itself too important and a more drastic method consists in considering a single- or a two-step mechanism [11–14], for which the computational expenses become minimal. In the present work, a single-step mechanism is considered. This mechanism is based on the notion of a virtual species, i.e., combustion products are lumped into a single fictive species hereafter denoted A_Φ, the thermodynamic properties of which are deduced from energy and mass conservation laws. Furthermore, the pre-exponential coefficient associated to the single-step Arrhenius law is optimized to restore the desired combustion characteristics. The introduction of such a virtual species has been already presented in the literature, see for instance references [11, 14]. In two of the aforementioned references [14, 15], a two-step chemistry was considered. This is in contrast with the present approach since the model we propose herein is based on an existing single-step model [11] constructed to restore the propagation properties of a flame. In the present work, this optimized single-step (OSS) model is designed to capture the most important characteristics of auto-ignition.

1.1. High activation energy asymptotic analysis

The auto-ignition of a homogeneous mixture between a fuel F and an oxidizer O is considered. At $t = 0$, the mixture is initially placed at the temperature T^u and follows an adiabatic and isobaric transformation. The superscripts u and b stand for the fresh reactants and burnt gases values, respectively. Assuming the variations of mass fraction of fuel and oxidizer to remain negligible before ignition proceeds, i.e., $Y_\mathrm{F} = Y_\mathrm{F}^u$ and $Y_\mathrm{O} = Y_\mathrm{O}^u$, the energy conservation equation is sufficient to fully characterize the evolution.

With a chemical kinetics represented through a single-step Arrhenius law, the energy equation can be recast as a temperature budget

$$\rho C_p \frac{dT}{dt} = Q\dot{\omega} \quad \text{with} \quad \dot{\omega} = K\rho Y_{\mathrm{F}}^u Y_{\mathrm{O}}^u \exp\left(-\frac{E_a}{RT}\right) \tag{1}$$

where Q, C_p, and ρ stand for the heat released per unit mass of fuel, the specific heat at constant pressure, and the density of the mixture, respectively. Here, $\dot{\omega}$ is the molar reaction rate (i.e., the fresh reactants consumption rate) and K is the pre-exponential factor.

Finally, the quantity E_a represents the activation energy, which can be expressed as a function of the activation temperature T_a as $E_a = RT_a$, where R stands for the perfect gas constant. According to this definition, the exponential term in Eq. (1) can be rewritten as

$$\exp\left(-\frac{T_a}{T}\right) = \exp\left(-\frac{T_a}{T^u} \cdot \frac{1}{1+\epsilon}\right) \tag{2}$$

where $\epsilon = (T - T^u)/T^u$ represents a small temperature increment. Within the standard high activation energy asymptotics, the description of the mixture evolution until auto-ignition takes place may indeed be restricted to very small variations of the temperature from its initial state. Thus, the term inside the exponential can be expanded as a function of the small parameter ϵ in such a manner that

$$\exp\left(-\frac{T_a}{T}\right) = \exp\left(-\frac{T_a}{T^u} \cdot (1 - \epsilon + \epsilon^2 - ...)\right) \tag{3}$$

which, after neglecting the higher-order terms, gives

$$\exp\left(-\frac{T_a}{T}\right) = \exp\left(-\frac{T_a}{T^u} \cdot (1-\epsilon)\right) = \exp\left(-\frac{T_a}{T^u} + \frac{T_a(T-T^u)}{(T^u)^2}\right) \tag{4}$$

In this respect, it should be pointed out that the above expression is often expressed in terms of the normalized parameter $\Theta = (T^u)^2/(T_a \cdot Q/C_p)$ and the non-dimensional temperature increment $\theta = (T - T^u)/(Q/C_p)$ as

$$\exp\left(-\frac{T_a}{T}\right) = \exp\left(-\frac{T_a}{T^u} + \frac{T_a Q/C_p}{(T^u)^2} \cdot \frac{T - T^u}{Q/C_p}\right) = \exp\left(-\frac{T_a}{T^u} + \frac{\theta}{\Theta}\right) \tag{5}$$

Thus, Eq. (1) can be recast as follows

$$\frac{d\theta}{dt} = K Y_{\mathrm{F}}^u Y_{\mathrm{O}}^u \exp\left(-\frac{T_a}{T^u}\right) \exp\left(\frac{\theta}{\Theta}\right) \tag{6}$$

This equation is then normalized in such a manner that

$$\frac{dy}{d\tau^*} = \frac{1}{\Theta}\exp\left(y\right) \tag{7}$$

where

$$\tau^* = \frac{t}{t_c} \quad \text{and} \quad y = \frac{\theta}{\Theta} \tag{8}$$

with a characteristic time scale

$$t_c = \frac{1}{KY_{\mathrm{F}}^u Y_{\mathrm{O}}^u}\exp\left(\frac{T_a}{T^u}\right) \tag{9}$$

Then, Eq. (7) becomes

$$\frac{dy}{\exp(y)} = \frac{d\tau^*}{\Theta} \tag{10}$$

and integration of Eq. (10) between 0 and τ^* leads to

$$\tau^* = \Theta\left(1 - \exp\left(-\frac{\theta}{\Theta}\right)\right) \tag{11}$$

A characteristic dimensionless time $\tau_i^* = \Theta$ can be identified. It corresponds to the ignition delay

$$\tau_i = \Theta \cdot t_c = \frac{\Theta}{KY_{\mathrm{F}}^u Y_{\mathrm{O}}^u}\exp\left(\frac{T_a}{T^u}\right) \tag{12}$$

The above expression shows that both the pre-exponential factor K and the activation temperature T_a (or activation energy E_a) are parameters upon which the optimization can be performed to recover the ignition delay. The reference ignition delay, thereafter denoted as $\tau_{i,0}$, can be obtained from either experimental data or by considering detailed chemistry computations.

1.2. OSS model

Within the OSS framework, the single reaction considered between a hydrocarbon $\mathrm{C_nH_m}$ and air $\mathrm{O_2}+\gamma\mathrm{N_2}$ as the oxidizer at any given equivalence ratio Φ is written as follows

$$\Phi \mathrm{C}_n\mathrm{H}_m + \left[n + \frac{m}{4}\right]\left(\mathrm{O}_2 + \gamma\mathrm{N}_2\right) \rightarrow \Phi A_\Phi + \gamma\left[n + \frac{m}{4}\right]\mathrm{N}_2 \tag{13}$$

The quantity A_Φ stands for the virtual species into which all the combustion products have been lumped. At this level, it is noteworthy that, in Eq. (13),

the consideration of a fuel containing nitrogen atoms (e.g., ammonia NH_3) will require only a slight modification since nitrogen should no longer be considered apart from the virtual species. In this case, the virtual species must indeed account not only for the atomic budgets of C, H, and O atoms, it must also incorporate the atomic budget of nitrogen atoms.

The thermodynamical properties of the virtual species are defined to ensure mass, enthalpy, and entropy conservation during its evolution from the fresh reactants towards equilibrium. Thus, the characteristics of the virtual species satisfy the following set of constraints

- Mass conservation

$$W_{A_\Phi} = W_{\mathrm{C}_n\mathrm{H}_m} + \frac{n + m/4}{\Phi} W_{\mathrm{O}_2} \tag{14}$$

  and hence,

$$Y_{\mathrm{A}_\Phi} = \left(\frac{r_s}{\Phi} + 1\right)\left[1 + \frac{r_s}{\Phi}\left(1 + \frac{\gamma W_{\mathrm{N}_2}}{W_{\mathrm{O}_2}}\right)\right]^{-1} \tag{15}$$

  The quantity $r_s = (n + m/4) \cdot W_{\mathrm{O}_2}/W_{\mathrm{C}_n\mathrm{H}_m}$ is the mass stoichiometric ratio.

- Enthalpy conservation

$$h_{A_\Phi}(T) = \frac{\sum_{k=1}^{N_s} Y_k h_k(T) - Y_{\mathrm{N}_2} h_{\mathrm{N}_2}(T)}{Y_{A_\Phi}} \tag{16}$$

- Entropy conservation

$$s_{A_\Phi}(T) = \frac{\sum_{k=1}^{N_s} Y_k s_k(T) - Y_{\mathrm{N}_2} s_{\mathrm{N}_2}(T)}{Y_{A_\Phi}} \tag{17}$$

In practice, the molar thermodynamic properties of the virtual species, namely the specific heat at constant-pressure, enthalpy, and entropy are represented with the standard seven-coefficient polynomials of Gordon and McBride [16]. These coefficients are presently tabulated as functions of the unburnt gases initial condition of pressure, and composition (temperature and species mass fractions) using the `Cantera` software [17]. Finally, within the OSS modeling framework, the molar reaction rate $\dot{\omega}^{\mathrm{OSS}}$ has been modified by following the procedure described in reference [11]. This procedure allows the determination of the pre-exponential factor K as a function of

the equivalence ratio Φ while avoiding some numerical difficulties associated to the reaction order. As explained in reference [11], it may be decomposed into two distinct steps : (i) a *remapping* step, which consists in the modification of the expression of the pre-exponential factor so that for any quantity presenting a bell shaped behavior (e.g., laminar flame speed or burnt gas temperature), the maximum reached around a given value $\Phi_{\max}$ is recovered, and (ii) a *rescaling* step that introduces a correction to fit a prescribed bell shaped curve given by a reference detailed chemical scheme or experimental data. The molar reaction rate in the OSS model is thus expressed as

$$\dot{\omega}^{\mathrm{OSS}} = K\rho\phi \left(\frac{Y_{\mathrm{F}} + Y_{\mathrm{O}}}{\phi Y_{\mathrm{F}} + Y_{\mathrm{O}}}\right)^2 Y_{\mathrm{F}} Y_{\mathrm{O}} \exp\left(-\frac{E_a}{RT}\right) \tag{18}$$

Here, $\phi = r_s Y_{\mathrm{F}}^{\infty}/Y_{\mathrm{O}}^{\infty}$, with Y_{F}^{∞} and Y_{O}^{∞} the mass fractions of fuel and oxidizer in their respective inlets, is a parameter that remains constant for any given values of the equivalence ratio Φ of the mixture.

1.3. Restoration of the laminar premixed flame velocity

The above expression of the single step chemistry model has been introduced to restore the laminar flame propagation velocity S_L^0. In fact, the laminar flame theory [18] allows to establish an explicit relationship between the laminar flame speed and the pre-exponential factor K_{P}

$$\begin{aligned} S_L^0 &= \frac{1}{\rho^u Y_{\mathrm{F}}^u} \int_{-\infty}^{+\infty} \dot{\omega}^{\mathrm{OSS}} dx \\ &= \frac{1}{\rho^u Y_{\mathrm{F}}^u} \int_{-\infty}^{+\infty} K_{\mathrm{P}}\rho\phi \left(\frac{Y_{\mathrm{F}} + Y_{\mathrm{O}}}{\phi Y_{\mathrm{F}} + Y_{\mathrm{O}}}\right)^2 Y_{\mathrm{F}} Y_{\mathrm{O}} \exp\left(-\frac{T_a}{T}\right) dx \end{aligned} \tag{19}$$

A subscript P has been added to the pre-exponential factor so as to emphasize that the corresponding values has been optimized to recover the propagation characteristics. A cost function CF is introduced [11]. It is based on a comparison against a reference value of the laminar flame speed $S_{L,ref}^0$ obtained using a detailed chemical scheme

$$\begin{aligned} \mathrm{CF}(\boldsymbol{K_{\mathrm{P}}}) &= \left\| S_L^0 - S_{L,ref}^0 \right\| \\ &= \left\| \frac{1}{\rho^u Y_{\mathrm{F}}^u} \int_{-\infty}^{+\infty} \boldsymbol{K_{\mathrm{P}}}\rho\phi \left(\frac{Y_{\mathrm{F}} + Y_{\mathrm{O}}}{\phi Y_{\mathrm{F}} + Y_{\mathrm{O}}}\right)^2 Y_{\mathrm{F}} Y_{\mathrm{O}} \exp\left(-\frac{T_a}{T^u}\right) - S_{L,ref}^0 \right\| \end{aligned} \tag{20}$$

In the above equation, the quantity in bold denotes the parameter to be optimized. The minimization problem for the pre-exponential factor K_{P}

is solved by using the Brent's algorithm [19]. Following this procedure, the values of K_{P} are tabulated as a function of the fresh mixture conditions P, T^u, and Φ. For each set of values (P, T^u, Φ), the resulting entry in the table contains 15 values (2×7 coefficients for the NASA polynomials plus the pre-exponential factor).

2. Extended OSS model

2.1. Ignition-optimized chemistry

Based on Eq. (12) and using the molar reaction rate expression given by Eq. (18), it is possible to reformulate the cost function CF to be minimized based on a comparison against a reference ignition delay $\tau_{i,0}$

$$\begin{aligned} \mathrm{CF}(\boldsymbol{K_{\mathrm{I}}}) &= \|\tau_i - \tau_{i,0}\| \\ &= \left\| \frac{(T^u)^2/(T_a \cdot Q/C_p)}{\phi \left(\frac{Y_{\mathrm{F}}+Y_{\mathrm{O}}}{\phi Y_{\mathrm{F}}+Y_{\mathrm{O}}}\right)^2 Y_{\mathrm{F}} Y_{\mathrm{O}}} \cdot \frac{1}{\boldsymbol{K_{\mathrm{I}}}} \exp\left(\frac{T_a}{T^u}\right) - \tau_{i,0} \right\| \end{aligned} \tag{21}$$

It should be noticed that in Eq. (21) a subscript I has been added to the pre-exponential factor. This is to emphasize that the value of K has been optimized to restore the value of the ignition delay. In order to minimize this cost function, the activation energy (or temperature) has been first estimated roughly so as to obtain ignition delay values of the same order of magnitude as those obtained with the reference chemical scheme. Then, the minimization problem for the pre-exponential factor K_{I} is solved using the same Brent's algorithm [19] as the one retained for the propagation-optimized model [11]. The resulting values of K_{I} are tabulated as a function of the fresh reactants conditions expressed in terms of operative pressure P, unburned gas temperature T^u, and equivalence ratio Φ. The entries of the table are therefore the same as those previously used, namely 15 values for each set of values (P, T^u, Φ). As an aside, it is noteworthy that a more complex optimization algorithm could be used to obtain a refined description of the temporal evolution of the temperature during ignition events. This is however at the price of a significant increase of CPU costs and additional modelling difficulties if applied to turbulent flow conditions (see Appendix A). Therefore, the corresponding algorithm has not been retained for the purpose of the present study.

This procedure is now applied to n-heptane/air combustion. The choice of this fuel is motivated by the fact that the n-heptane stands as one of the

primary reference fuels (PRF). It is characterized by an octane rating of zero reflecting its high sensitivity with respect to ignition. Moreover, this mixture has been previously studied and is well documented in the literature [20, 21]. The chemical mechanism used to obtain the reference ignition delay (hereafter referred to as REF), is the one of Patel *et al.* [22] which has been extensively validated for computations in engine conditions. It contains 29 chemical species and 52 elementary reaction steps.

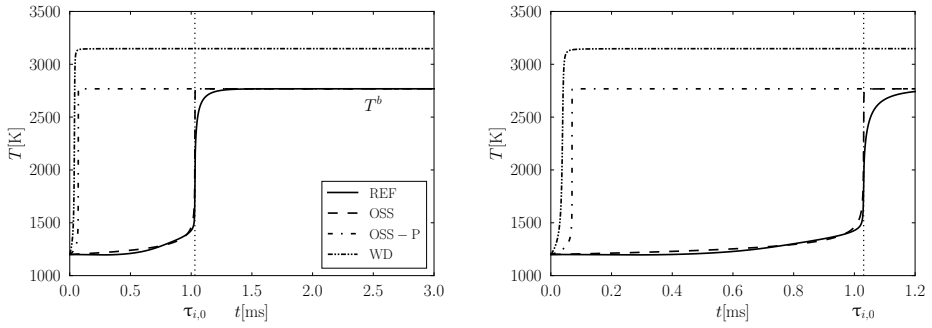

Fig. 1. Comparison between temperature temporal evolutions obtained with single-step chemistry models and the reference chemistry (REF) for a stoichiometric n-heptane/air mixtures with $T^u = 1200$ K and $P = 5$ bar.

A stoichiometric mixture of n-heptane/air at $P = 5$ bar and $T^u = 1200$ K is considered. Figure 1 reports a comparison between the responses of three distinct single-step models compared to the reference chemistry (REF). In this figure, WD denotes the single-step model of Westbrook and Dryer [23], OSS-P refers to the optimized single-step model that has been introduced in reference [11] to recover the laminar premixed flame characteristics, and OSS refers to the present proposal. From this figure, it is quite clear that both the WD and OSS-P models are unable to recover a relevant estimate of the ignition delay. In comparison with the WD chemistry, the OSS-P model leads to an excellent estimate of the burned gases temperature. However, only a (very) slight improvement of the ignition delay prediction is obtained by using the OSS-P model: in comparison with the REF chemistry, the error remains larger than one order of magnitude. This is in contrast with the results obtained with the new version of the OSS model. Indeed, the two main features, namely the ignition delay $\tau_{i,0}$ and the burnt gas temperature T^b, are perfectly restored when comparing the results of the OSS model against the reference chemistry. However, some residual differences

may be observed. For instance, the temporal evolution obtained with the OSS model follows a classical single-step Arrhenius law and it does not account for any changes in the steepness of the evolution. This can lead to either an overestimation or an underestimation of the temperature during the reactive mixture evolution, which may be associated to changes in the production and consumption rates of radicals during the initiation period. Furthermore, once ignition takes place, the temperature evolution is very abrupt until the equilibrium state is reached. Thus, the effect of termination reactions like recombination reaction or decomposition are not taken into account. The purpose of the OSS model is to recover the two main properties mentioned above ($\tau_{i,0}, T^b$) using a single-step representation.

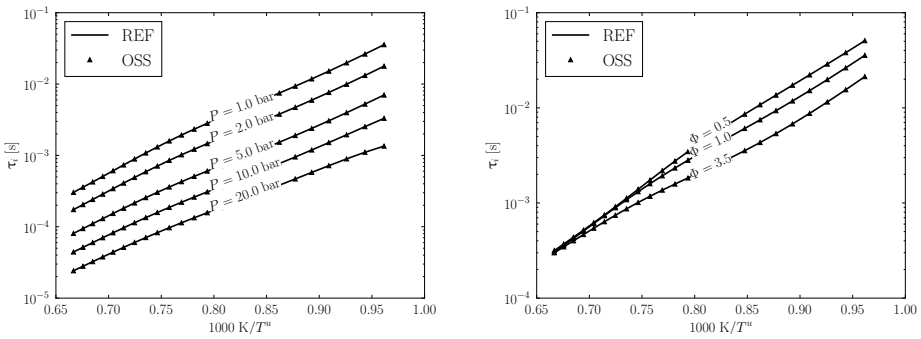

Fig. 2. Comparison between ignition delays obtained with `Cantera` using OSS and reference values obtained with REF chemistry [22] for a stoichiometric n-heptane/air mixture at various pressure levels (left) and at atmospheric pressure for various equivalence ratio (right).

Figure 2(a) reports a comparison of ignition delays obtained with the OSS model against the reference mechanism for different initial pressure and temperature levels for a stoichiometric mixture. The reference values of the ignition delay are well reproduced for all the considered conditions. A similar behavior is obtained as a function of the equivalence ratio as shown in Figure 2(b). It can be noticed that the temperature levels under consideration are relatively large. In fact, at lower temperatures, cool flame phenomena [21, 22], for which ignition takes place within a two-stage oxidation process, may appear. The corresponding phenomena are mostly observed for heavy hydrocarbon fuels. The nature of the single-step reaction imposes a strictly increasing evolution of temperature, and it is thus difficult to reproduce such a two-stage behavior with the present model.

2.2. Coupling between the propagation and ignition models

The objective of the present section is to study the possibility of reproducing both the laminar flame propagation and the ignition characteristics using the OSS framework. On the one hand, our previous work has established its capability to reproduce the main features of laminar premixed flames (burned gases temperature, flame propagation velocity and thickness). Moreover, it must be emphasized that the influence of stretching has been also studied by performing one-dimensional strained diffusion flames computations [11] and, when compared to the reference detailed chemistry results, the OSS showed excellent performance in comparison to other reduced chemistry models available in literature. On the other hand, the previous section has established that the OSS framework is also a good candidate to recover ignition characteristics provided that the optimization step is based on ignition properties taken as a reference. The objective is now to take advantage of both optimization procedures to end up with a single combination of both OSS models, which allows to reproduce not only ignition but also laminar flame propagation properties. The coupling is achieved through the determination of the pre-exponential factor as a function of the corresponding values obtained for both the propagation and ignition models. To this end, the expression of the resulting value is evaluated as follows

$$K_{\mathrm{PI}} = K_{\mathrm{P}} + \frac{K_{\mathrm{I}} - K_{\mathrm{P}}}{2}\left[1 + \tanh\left(\frac{T^u - T_c}{\sigma}\right)\right] \tag{22}$$

Here, the subscript PI stands for the coupled model for propagation and ignition. This expression is inspired by the work of Misdariis *et al.* [15]. Nevertheless, in contrast with this previous study, the temperature used for the differentiation of both combustion modes is not the local temperature T but the unburnt mixture temperature T^u. In fact, considering the local temperature T may allow to follow the transition between auto-ignition and premixed flame propagation. However, this behavior is deemed too complex to be restored with a single-step model, and hence, only the combustion mode associated with the unburnt gas temperature T^u is considered. Moreover, it should be acknowledged that the use of Eq. (22) just aims at obtaining a smooth transition between the pre-exponential factor value relevant to laminar flame propagation (i.e., K_{P}) and the one relevant to ignition processes (i.e., K_{I}). This transition requires the value of the parameter σ to be specified and all the numerical simulation results that will be presented herein have been obtained with $\sigma = 20$ K. In this respect, it is also necessary to express the cross-over temperature T_c, which is involved in Eq. (22). As

shown in Appendix B, it can be deduced from the H_2/O_2 sub-mechanism, which can be thought as the kernel of any hydrocarbon chemistry. The value of the cross-over temperature T_c is not a constant [24, 25]. It depends mostly on the pressure and it can be determined prior to the simulation. At this level, it must be emphasized that the whole set of computations have been conducted using the coupled model as given by Eq. (22). In this respect, it is also noteworthy that the values of the two functions

$$K^* = \frac{K_{\mathrm{PI}} - K_{\mathrm{P}}}{K_{\mathrm{I}} - K_{\mathrm{P}}} \qquad \text{and} \qquad 1 - K^* = \frac{K_{\mathrm{I}} - K_{\mathrm{PI}}}{K_{\mathrm{I}} - K_{\mathrm{P}}} \tag{23}$$

can be thought as weighting factors between the *"ignition mode"* and the *"propagation mode"*, respectively.

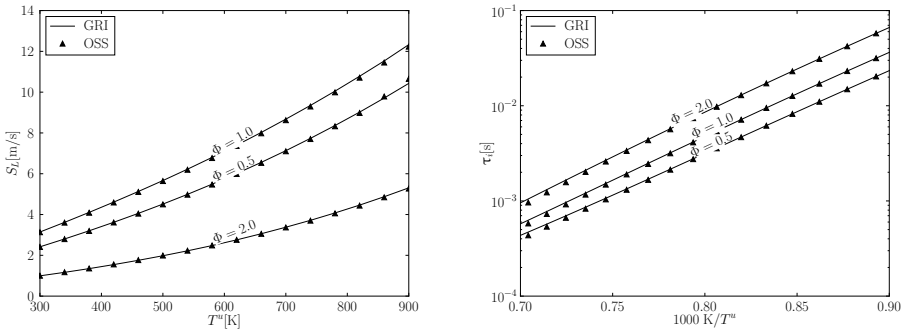

Fig. 3. Comparison between the laminar flame speed (left) and ignition delay (right) obtained with the reference mechanism and the OSS model for methane-oxygen mixtures in different conditions.

The capability to reproduce both combustion modes must now be established. In Fig. 3, the performance of the coupled model is assessed using the `Cantera` software for a methane/oxygen mixture. The choice of this fuel is motivated by the fact that methane has been widely used to analyze both auto-ignition and propagation of one-dimensional laminar premixed flames (e.g., references [26, 27]). The reference mechanism retained to describe its chemistry is the GRI3.0 hereafter denoted GRI [28]. In Fig. 4 is depicted the evolution of the weighting function K^* over the whole range of temperature that is considered in Fig 3. The level of agreement obtained between the results issued from the OSS model and those from detailed chemistry is excellent (see Fig. 3).

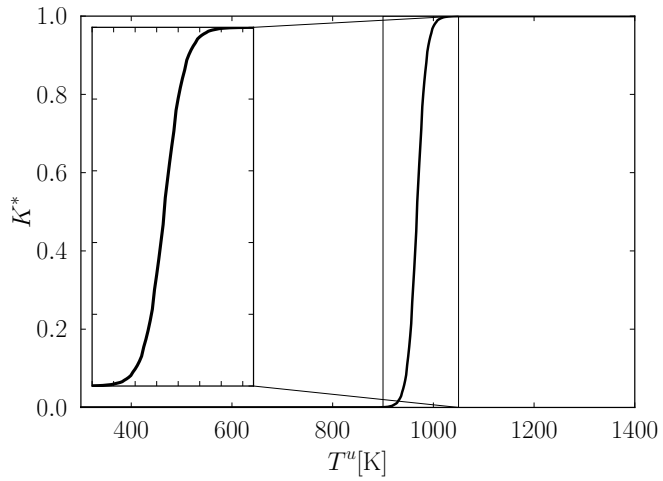

Fig. 4. Evolution of the weighting function K^* for $\Phi = 1$ over the range of temperature considered in Fig 3, on the left: zoom a reduced range of temperature [900 K : 1050 K].

2.3. Efficient data query

In practical applications, i.e., CFD applications, the values of the pre-exponential factor and thermodynamic coefficients are stored in a table. During the computation, it is possible to query the table to recover the corresponding properties of the virtual species by considering the local conditions at any point of the domain. For the sake of efficiency in terms of both memory space and access time, it is necessary to optimize the number of entries in the table. Furthermore, the retained number of entries must properly account for regions featuring large variations. For instance, when considering the local composition, presently represented by the mixture fraction ξ, the largest variations of the characteristic properties of combustion (e.g., flame speed, ignition delay, burnt gases temperature) are concentrated around the stoichiometric mixture fraction ξ_{st} or the most reactive mixture fraction ξ_{mr}. Thus, a sufficiently refined discretization is required in the vicinity of the corresponding values. On the contrary, far from these values, a smaller number of points is required since the variations of the characteristic properties remain small. A common practice consists in retaining an homogeneous discretization of the mixture fraction using a sufficiently small step $\Delta\xi$. This method guarantees a good discretization in the high-variation zones while being easy to access. As a matter of fact, for any physical value

ψ and its corresponding tabulated values $\psi[i_\xi]$, with i_ξ varying from 0 to $N_\xi - 1$ (N_ξ being the number of points retained to discretize the mixture fraction space so that $\Delta\xi = 1/N_\xi$), given a local value of ξ, the tabulated propertie ψ can be directly calculated as

$$\psi = \psi\left[i_\xi\right] + \left(\xi/\Delta\xi - i_\xi\right) \cdot \left(\psi\left[i_\xi + 1\right] - \psi\left[i_\xi\right]\right) \tag{24}$$

where $i_\xi = \lfloor \xi/\Delta\xi \rfloor$. Here, the symbol $\lfloor . \rfloor$ denotes the `floor` function. Thus, no research algorithm, which induces an additional computational cost, is needed to find the index of the tabulated value.

However, this method may induce a large table since the discretization step must be small enough to account for the variations of the physical properties. Therefore, a new tabulation method benefiting from both direct access and reduced size is presented below. This method is based on the use of power and hyperbolic functions.

2.3.1. Change of coordinates

Since the stoichiometric mixture fraction is usually shifted towards small values, a rescaled mixture fraction $\widehat{\xi}$ is first introduced in such a manner that

$$\widehat{\xi} = \xi^{\ln(0.5)/\ln(\xi_c)} \tag{25}$$

where $\xi_c = \xi_{st}$ is the targeted center of the discretization for the normalized mixture fraction. The most reactive mixture fraction ξ_{mr} can be also retained as the targeted value ξ_c. This rescaling step allows the centering of the stoichiometric (or most reactive) mixture fraction at the middle of the variation range. Furthermore, a symmetric discretization with respect to ξ_c can be retained. With such a procedure, the numerical difficulties associated with the evaluation of small values of the mixture fraction can be circumvented. Finally, it should be emphasized that the mixture fraction can be straightforwardly reconstructed from the rescaled mixture fraction as $\xi = \widehat{\xi}^{\ln(\xi_c)/\ln(0.5)}$.

2.3.2. Refinement function

The second step consists in the discretization of the domain of variation of the rescaled variable $\widehat{\xi}$ using a refinement function f. This function is defined on the interval $[0, 1]$ as

$$f(\widehat{\xi}) = \widehat{\xi}_c \left(1 + \frac{\sinh(\beta(\widehat{\xi} - \alpha))}{\sinh(\beta\alpha)}\right) \tag{26}$$

where β denotes the stretching parameter ($\beta > 1$) and the value of α is given by

$$\alpha = \frac{1}{2\beta} \ln \left(\frac{1 + (e^{\beta} - 1) \cdot (\widehat{\xi}_c / \widehat{\xi}_d)}{1 + (e^{-\beta} - 1) \cdot (\widehat{\xi}_c / \widehat{\xi}_d)} \right) \tag{27}$$

Here, $\widehat{\xi}_c$ and $\widehat{\xi}_d$ denote respectively the centering value around which the refinement must be performed, and the range of variations of $\widehat{\xi}$, respectively. Based on Eq. (25), $\widehat{\xi}_c = 0.5$; and, by construction, $\widehat{\xi}_d = 1$. Under these conditions, $\alpha = 0.5$ is obtained. Indeed, Eq. (27) can be simplified to

$$\begin{aligned} \alpha &= \frac{1}{2\beta} \ln \left(\frac{1 + (e^{\beta} - 1)/2}{1 + (e^{-\beta} - 1)/2} \right) = \frac{1}{2\beta} \ln \left(\frac{e^{\beta} + 1}{e^{-\beta} + 1} \right) \\ &= \frac{1}{2\beta} \ln \left(\frac{e^{\beta/2} \cdot (e^{\beta/2} + e^{-\beta/2})}{e^{-\beta/2} \cdot (e^{-\beta/2} + e^{\beta/2})} \right) = \frac{1}{2\beta} \ln \left(\frac{e^{\beta/2}}{e^{-\beta/2}} \right) = \frac{1}{2\beta} \ln \left(e^{\beta} \right) = \frac{1}{2} \end{aligned} \tag{28}$$

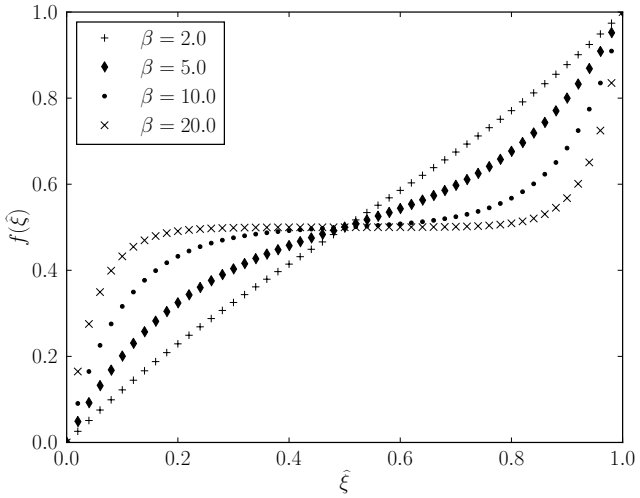

Fig. 5. Refinement function obtained for different values of β.

Figure 5 displays the influence of the parameter β on the function f for a given discretization step $\Delta\widehat{\xi}$. It shows that, depending on the value of β, the above discretization leads to either (i) linear or (ii) non-linear distributions featuring a high concentration of points around the targeted value $\widehat{\xi}_c = 0.5$.

The expression of the refinement function leads to an explicit relationship between the linearly-discretized values and the refined ones through the following inverse function.

2.3.3. Inverse refinement function

The function f can be inversed and f^{-1} is expressed as

$$f^{-1}(\widehat{\xi}) = \alpha + \frac{1}{\beta}\text{arsinh}\left(\sinh(\beta\alpha)\cdot(\widehat{\xi}/\widehat{\xi_c} - 1)\right) \tag{29}$$

From the application of the inverse function, and based on the knowledge of $\Delta\widehat{\xi}$, the index i_ξ is readily obtained as

$$i_\xi = \left\lfloor \frac{f^{-1}(\widehat{\xi})}{\Delta\widehat{\xi}} \right\rfloor = \left\lfloor \frac{f^{-1}\left(\xi^{\ln(0.5)/\ln(\xi_c)}\right)}{\Delta\widehat{\xi}} \right\rfloor \tag{30}$$

which avoids any resort to sorting algorithms, a rather expensive procedure in terms of CPU costs.

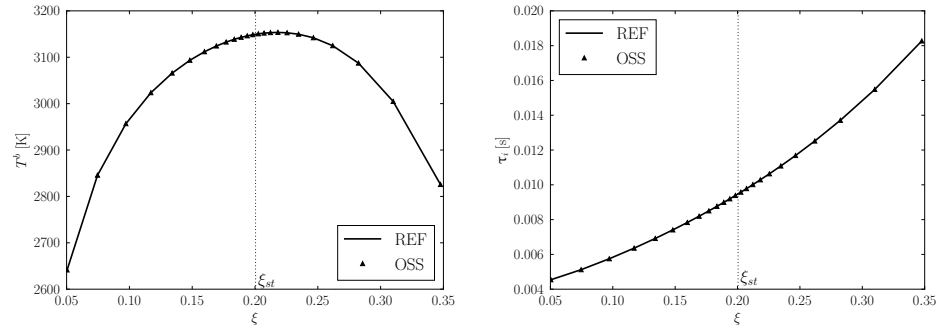

Fig. 6. Application of the refinement function with $\beta = 10$ to describe the burnt gas temperature T^b (left) and the ignition delay τ_i (right) as a function of the mixture fraction ξ. Methane/oxygen combustion at atmospheric pressure and initial temperature $T^u = 1200$ K.

2.3.4. Application of the optimized discretization

Figure 6 illustrates the application of the refinement function to the auto-ignition of a methane/oxygen mixture at atmospheric pressure and initial temperature $T^u = 1200$ K. As expected, expressed as a function of the mixture fraction, the burnt gas temperature displays a characteristic bell-shaped evolution. The maximum is located in the vicinity of the stoichiometric mixture fraction ξ_{st}. Thus, by retaining the stoichiometric condition

as the targeted value, it is possible to achieve a good discretization of this region which displays the largest curvature. Even if it is less noticeable, the strongest curvature of the ignition delay function is also located around the stoichiometric condition. However, if needed, changing the value of ξ_c allows to shift the refinement around a different condition.

3. Application of the OSS model to DNS computations

The performance of the resulting model is further assessed from direct numerical simulations (DNS) applications. Four distinct configurations are selected with an increasing level of complexity: (i) an homogeneous reactor, the two-dimensional evolution a non-homogeneous mixture (ii) in laminar conditions and then (iii) in homogeneous isotropic turbulence (HIT), and finally (iv) the development of a flame kernel in heterogeneous auto-ignitive conditions. The purpose of these simulations is to use the chemistry model in the case of more realistic reactive flow fields. It should be pointed out that, even though these validation cases may be thought as relatively simple, they provide a unique opportunity for a deep analysis of the underlying physical assumptions and their possible impact on the results. Computations are carried out using the DNS solver `Asphodele` [29]. This solver, the main features of which have been already presented elsewhere (e.g., [29]), is based on a dilatable low-Mach number framework. Spatial derivatives are evaluated on regular meshes by making use of high-order precision finite difference schemes while time integration is carried out with a minimal storage third-order explicit Runge–Kutta scheme. The pressure-velocity coupling is handled within a standard projection-correction framework using the `HYPRE` library [30, 31]. Chemical source terms are evaluated using the SUNDIALS `CVODE` solver [32].

3.1. Homogeneous reactor

To avoid any other effects of molecular diffusion or convection on auto-ignition phenomena, a homogeneous isobaric reactor configuration has been considered as a preliminary test case. Thus, this configuration is a verification step to corroborate the correct implementation of the model in the DNS solver. Figure 7 displays the temporal evolution of the temperature obtained using both the OSS model and the reference chemistry for a stoichiometric n-heptane/air mixture at atmospheric pressure together with the corresponding temporal evolution of the dimensionless temperature $\theta = (T - \min(T))/(\max(T) - \min(T))$.

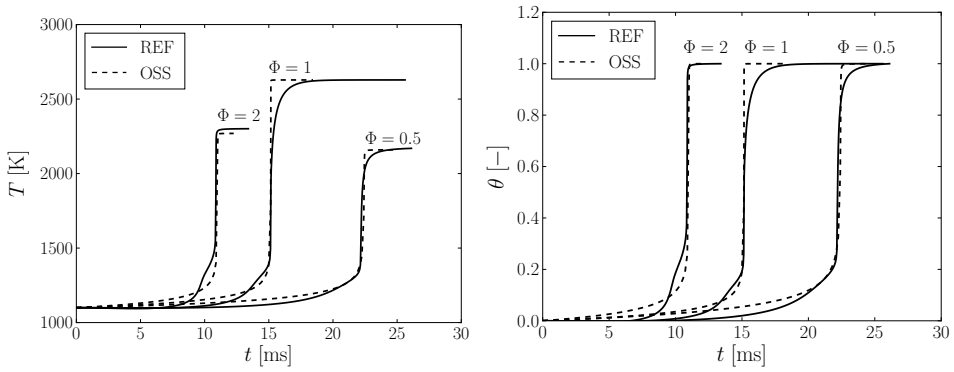

Fig. 7. Comparison of temperature T (left) and dimensionless temperature θ (right) temporal evolutions with OSS and reference chemistry for lean ($\Phi = 0.5$), stoichiometric ($\Phi = 1$), and rich ($\Phi = 2$) n-heptane/air mixtures at $T^u = 1200$ K.

As expected, the ignition delay is well recovered. However, some differences appear between the two models, which may be readily explained by the presence of intermediate chemical species in the reference model based on a more detailed chemistry. In fact, before ignition takes place, radicals are produced in large amounts [33]. These radical species feature different properties, which can modify the steepness of the temperature evolution. Due to the single-step nature of the OSS model, such changes in steepness cannot be reproduced. However, the main features of the auto-ignition profile, i.e., the ignition delay and burnt gases temperature, are satisfactorily reproduced. Thus, the use of the OSS model is expected to offer a cost-effective approach to solve chemistry in complex flows. Especially, it should allow to recover the early development of ignition spots at the right spatial location.

3.2. Two-dimensional configuration

In order to study more complex and relevant conditions, simulations of a two-dimensional heterogeneous n-heptane/air mixture were carried out. To do so the computational domain ($\mathcal{D}$) is discretized with 120 points in each direction and its dimensions are $L_{x_1} = L_{x_2} = L = 2$ mm. Pressure is held constant and equal to 5 bar. The composition field is initialized from the distribution of a normalized scalar ζ, which is described by a characteristic length scale $l_\zeta = 0.25$ mm (i.e. approximately $L/8$) and its distribution, i.e., its probability density function (PDF) is approximated by a beta function, which is defined from its first two moments: the mean value

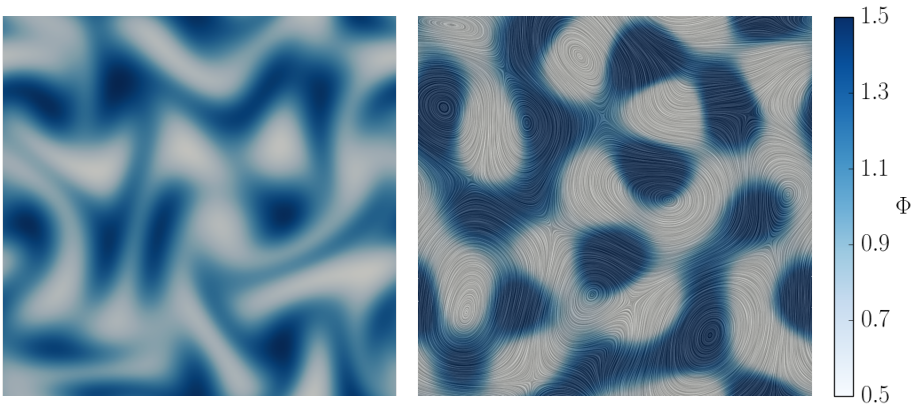

Fig. 8. Equivalence ratio fields at the initial time for the laminar case (left) and the HIT case (right).

$\overline{\zeta} = 0.5$ and the segregation-rate $S_\zeta = \overline{\zeta'^2}/\overline{\zeta}(1-\overline{\zeta}) = 0.2$. Further details concerning the scalar field initialization procedure can be found in reference [34]. Different flow-conditions are considered: ignition development in a fluid with no motion (laminar conditions) and ignition development in homogeneous isotropic turbulence (HIT). In the first case (i.e., laminar conditions), the heterogeneities are obtained from the preliminary simulation of a non-reactive heterogeneous composition mixture in an HIT flow field. This non-reactive simulation is performed until the desired composition range is obtained, namely an equivalence ratio ranging between $\Phi_{min} = 0.5$ and $\Phi_{max} = 1.5$. This preliminary step allows to generate: (i) a large range of composition gradients and (ii) multiple fuel-rich regions, each one featuring different values of the equivalence ratio. Hence, in each of these regions, the mixture is expected to ignite at a different time. At the end of this initialization procedure, the flow field is canceled (a zero-velocity condition is imposed) and chemistry is enabled. The resulting equivalence ratio field is depicted in Fig. 8(a). For the HIT case, Fig. 8(b) displays the equivalence ratio field superimposed on the velocity streamlines. The equivalence ratio field is renormalized in such a manner so that its variations remain bounded within the range $[0.5, 1.5]$.

3.2.1. Laminar conditions with non-homogeneous composition

The initial temperature is set to a value of 1200 K, which has been chosen in such a manner that, whatever the local value of the equivalence ratio Φ, only the *"ignition mode"* is triggered, i.e., $K^*(\boldsymbol{x}, t) = 1$. The simulations are

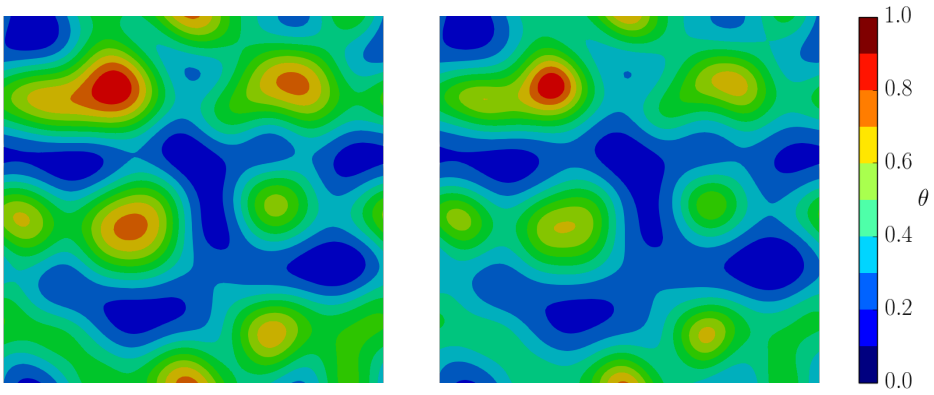

Fig. 9. Iso-values of the dimensionless temperature θ at $t^* = 0.82$ (laminar case). Left: REF chemistry. Right: OSS model.

carried out until the early stages of auto-ignition. In terms of the reduced time, it corresponds to $t^* = t/\tau_{i,0}^{mr} = 0.82$, where $\tau_{i,0}^{mr}$ stands for the reference ignition delay of the most reactive mixture fraction, i.e., the richest one in the present case (as deduced from preliminary computations of homogeneous reactors). It can be noted that, as pointed out in reference [35], the gradients of composition may induce some modifications in the ignition of the non-homogeneous mixtures with respect to homogeneous reactor computations. Thus, it is expected that the first spot does not ignite precisely at $t^* = 1.0$. However, the value of $\tau_{i,0}^{mr}$ provides an appropriate time scale to analyze the problem and it is therefore the one retained in the present study. Figure 9 displays the resulting field of the dimensionless temperature θ just before the auto-ignition of the first spot. It can be noted that the location of the first igniting spot is correctly predicted with the OSS model. Moreover, the location of the following igniting spots are also well reproduced. However, it can be observed that, even if the shapes of these spots are similar, their intensities display some slight differences when comparing the OSS model and the REF chemistry model. This can be explained by the steepness of the OSS model relative to the REF chemistry model. In fact, as discussed above for the homogeneous reactor, the production and consumption of radicals create differences in the steepness of the temperature evolution. The single-step nature of the OSS model results in more intense ignition spots. However, the detection of the most-reactive regions at the correct time, i.e., the one given by the multi-step chemistry computation, appears as a quite satisfactory result.

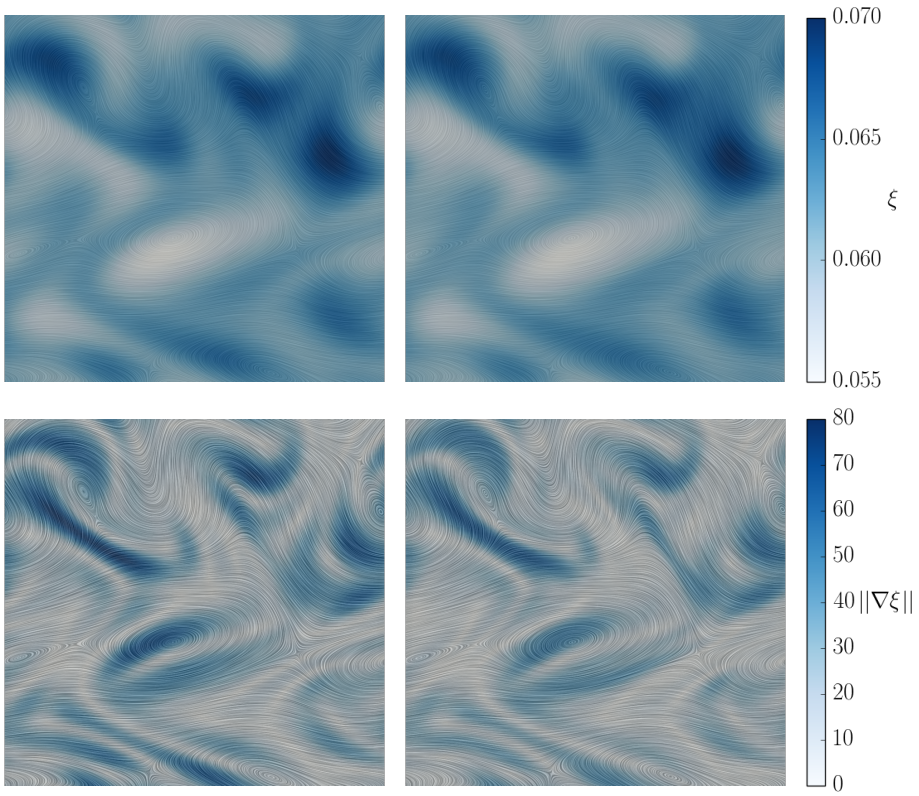

Fig. 10. Snapshots of the composition fields superimposed on the streamlines at $t^* = 0.94$ (HIT case). Top: mixture fraction ξ. Bottom: norm of the mixture fraction gradient $||\nabla\xi||$. Left: REF chemistry. Right: OSS model. SI units.

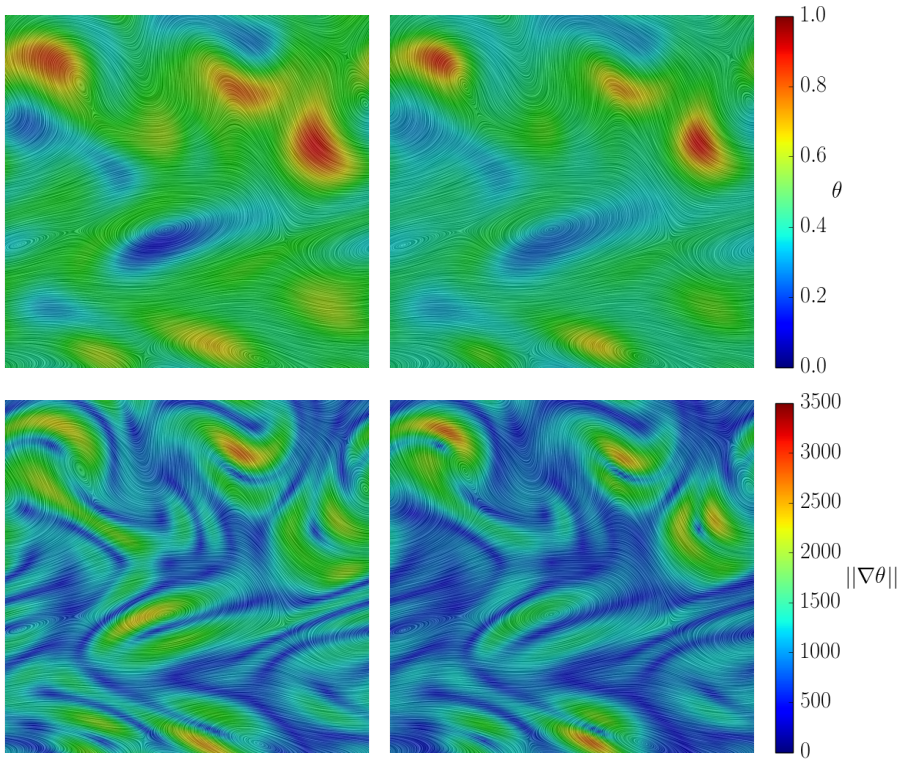

Fig. 11. Snapshots of the temperature fields superimposed on the streamlines at $t^* = 0.94$ (HIT case). Top: dimensionless temperature θ. Bottom: norm of the dimensionless temperature gradient $||\nabla\theta||$. Left: REF chemistry. Right: OSS model. SI units.

3.2.2. Homogeneous isotropic turbulence with non-homogeneous composition

In a second step of this study, the performance of the OSS model is evaluated in homogeneous isotropic turbulence (HIT) in order to test the proposed model in a more realistic flow field. The turbulent fluctuating velocity field is generated on the basis of the Rogallo's procedure [36] according to a Passot–Pouquet spectrum [37]. The integral length scale is set to $l_T = 0.3$ mm (i.e., approximately $L/6$) and the initial root mean square (RMS) of velocity fluctuations is set to $u_{\mathrm{RMS}} = 1.2$ m.s^{-1}. Again, the initial temperature is set to a value of 1200 K. As in the previous section, a dimensionless time $t^* = 0.94$ corresponding to the early stages of auto-ignition is chosen for the analysis. Figure 10 provides an illustration of the effect of the OSS model on the mixture fraction field and on its gradient. It can be pointed out that these flow fields are almost identical in both cases. Concerning the mixture fraction, it can be observed that the use of the OSS model has almost no consequence on the quality of the agreement obtained with the results issued from the REF chemistry. This behavior is expected since the mixture fraction stands as a passive scalar. Therefore, it is not directly altered by the reaction rate prediction but only through the variations of density and diffusivity. As a matter of fact, this dependency is more remarkable when looking at the field of the mixture fraction gradient where the gradient is indeed stronger near the auto-ignition spots (depicted below) and smaller elsewhere. This shows that the differences in the temperature evolution lead to variations of density that modify only slightly the evolution of the mixture fraction field.

Figure 11 reports a comparison between the normalized temperature and the normalized temperature gradient fields obtained with both the REF chemistry and the OSS model. Both temperature fields exhibit close characteristics. It can be observed that even though the first two ignition spots have been convected and stretched by the turbulent flow field, they are located in the same regions and display similar intensities. However, as emphasized above, the temperature steadily increases with the OSS model until ignition takes place and, as a consequence, the steepness of the evolution of the temperature field is found difficult to reproduce. Indeed, it can be seen that the gradient of temperature is stronger near the auto-ignition spots and milder elsewhere. This can be explained by the higher steepness in the evolution of temperature due to the single-step nature of the OSS model.

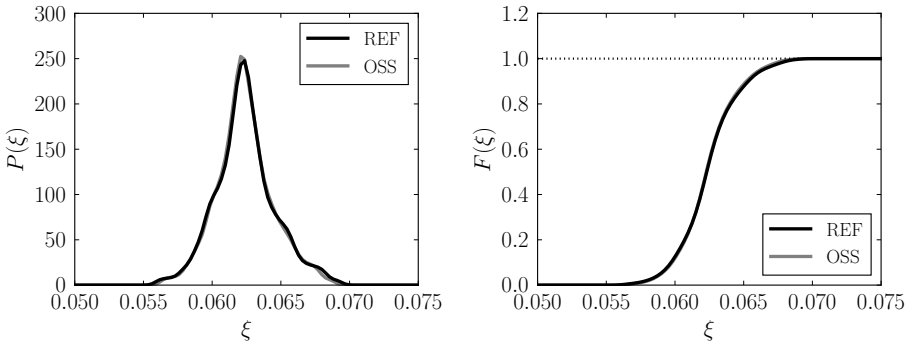

Fig. 12. Distribution functions of the mixture fraction for both the REF chemistry and the OSS model. Right: PDF. Left: CDF.

In order to provide a more quantitative analyses of the performance of the OSS model, statistical analysis are presented below. The distributions of the mixture fraction, namely the probability density function (PDF) and the cumulative density function (CDF), are reported in Fig. 12. As previously observed in the corresponding fields of Fig. 10, the use of the OSS model does not seem to alter the mixture fraction distribution.

However, as reported in Fig. 13, by considering the mixture fraction PDF in the form of different bins, some dissimilarities are put into evidence. For instance, the limiting values of the mixture fraction are slightly affected. Indeed, in the present case the most reactive mixture fraction also corresponds to the largest mixture fraction value. It is therefore the region where the impact of the temperature is the most important. Thus, the last bin is almost no longer represented with the OSS model since diffusivity variations start to take place. In a similar way, the smallest mixture fraction corresponds to the slowest igniting point. Since the temperature steadily increases when using the OSS model, even for the mixture fraction values which correspond to the slowest ignition, the differences in the temperature evolution may induce higher overall diffusivity, and hence, this may have an impact on the distribution of the mixture fraction.

The CDF of the norm of the mixture fraction gradient is depicted in Fig. 14. Both distributions are similar. However, the resulting CDF displays a sharper increase with the OSS model. In fact, as observed in the

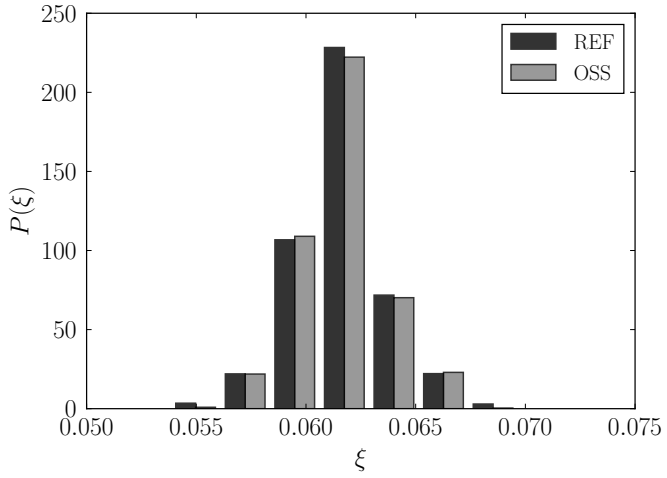

Fig. 13. Statistical approximation of the mixture fraction PDF. Black columns: REF chemistry. Grey columns: OSS model.

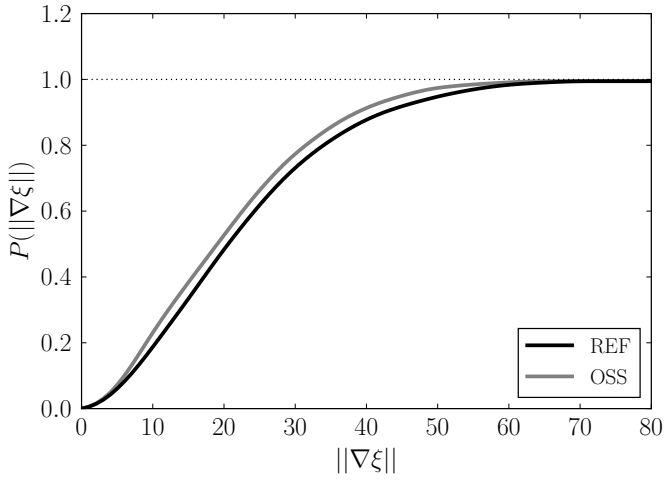

Fig. 14. Cumulative distribution function of the norm of the mixture fraction gradient for both the REF chemistry and the OSS model. SI units.

corresponding PDF, which is reported in Fig. 15, there is a higher representation of the smaller bins with the OSS model compared to the REF chemistry. This confirms that the overall temperature increase observed with the OSS model slightly modifies the transport, and thus increases the mixing rate.

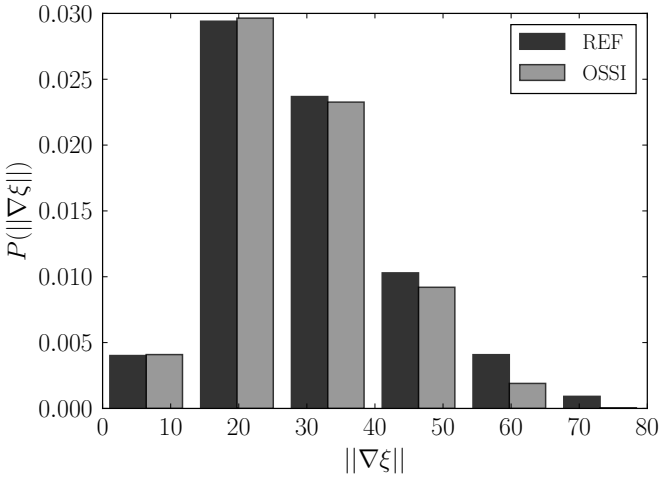

Fig. 15. Statistical approximation of the PDF of the norm of the mixture fraction gradient. Black columns: REF chemistry. Grey columns: OSS model. SI units.

A more pronounced effect may be expected for the dimensionless temperature gradient. Indeed, more significant differences do appear between the CFD of the dimensionless temperature gradient obtained with (i) the REF chemistry and (ii) the OSS model as reported in Fig. 16. It can be observed that on the one hand the slope has been slightly modified and on the other hand the statistical evolution takes place earlier. Figure 17 shows the corresponding PDF of the dimensionless temperature gradient. There is a higher representation of the bins for the smaller gradients in the OSS configuration. As discussed above, this is the imprint of the overall temperature increase observed with the OSS model active even in the least reactive zones. However, in contrast with the behavior observed for the mixture fraction gradient, there is still a non negligible persistence of the effects of the strongest gradients. This corresponds to the auto-ignition spots and their corresponding sharp increase of temperature obtained with the OSS model once auto-ignition starts.

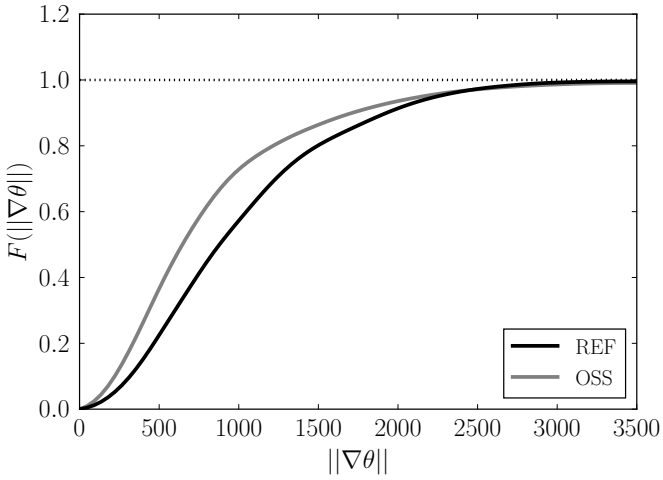

Fig. 16. Cumulative distribution function of the norm of the dimensionless temperature gradient for both the REF chemistry and the OSS model. SI units.

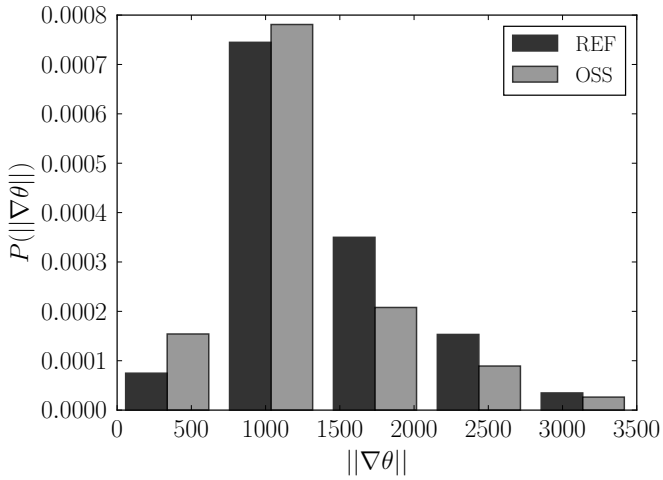

Fig. 17. Statistical approximation of the PDF of the norm of the dimensionless temperature gradient. Black columns: REF chemistry. Grey columns: OSS model. SI units.

Despite the small differences observed between the results obtained with the OSS model and those from the REF chemistry, the reduced cost of OSS chemistry makes the model appealing for the simulation of complex reactive flows fields for which the cost of a detailed chemistry calculation remains unaffordable and the availability of semi-detailed schemes limited. Finally, it is noteworthy that, for this set of conditions, the CPU time required to perform 100 iterations is 1368 s for the REF skeletal chemistry and 139 s for the OSS chemistry[1]. A ten factor gain in performance is thus achieved with the OSS model, which therefore appears as an excellent candidate for forthcoming three-dimensional numerical simulations of unsteady reactive flows in complex geometries. It should be also emphasized that this gain factor may be considerably larger if the comparison is performed with a more detailed mechanism including hundreds (or thousands) of chemical species and thousands of elementary reactions [3].

3.2.3. Flame kernel development in heterogeneous auto-ignitive conditions

Finally, the manuscript ends with the brief presentation of an application to a more complex configuration in which both "ignition" and "propagation" modes are triggered. Reactive mixtures of methane with air are considered for this last test case with the GRI mechanism [28] retained as a relevant detailed chemical description (i.e., REF chemistry). The initialization of the mixture fraction and velocity fields is the same as the one considered in the previous subsection. Thus, the HIT is again characterized by an integral length scale $l_T = 0.3$ mm and the initial root mean square (RMS) of velocity fluctuations is $u_{\mathrm{RMS}} = 1.2$ m.s^{-1}. The same value as the one retained in the previous subsection is also kept for the pressure, i.e., it is 5 bar.

In a first step of the computation, a turbulent flame kernel is developped, see Fig. 18. The retained procedure is as follows: at time $t^+ \equiv t/\tau_L^0 = 0.0$ — with $\tau_L^0 = \delta_L^0/S_L^0$ the stoichiometric premixed flame transit time — a perfectly-ignited flame kernel is initialized in the center of the computational domain [11, 31]. The species mass fractions and temperature profiles associated to this initial flame kernel are deduced from the preliminary computation of a one-dimensional laminar unstrained premixed flame performed with Cantera. This initialization procedure is exactly the same as the one previously retained by Er-Raiy et al. [11] and Zhao et al. [31], and

[1]These results where obtained in a local 40-cores working station. The processors are Intel(R) Xeon(R) CPU E5-2650 v4 @ 2.20GHz.

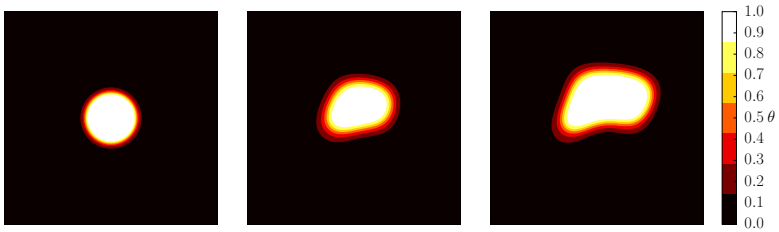

Fig. 18. Flame kernel development obtained with the REF chemistry. Left: $t^+ = 0.0$, middle: $t^+ = 0.9$, and right: $t^+ = 1.8$.

the interested reader may found further details about it in the corresponding references. During this first step of the computation, the temperature in the fresh reactants is uniform and set to 700 K. The corresponding temperature level is below the crossover and, as a consequence, only the "propagation mode" is triggered. The values of K_{P} however display some local variations, which are associated to equivalence ratio variations in the fresh reactants (see the left side of Fig 19).
Once initialized, the flame kernel is developped until $t^+ = t_f^+ = 1.8$. The same procedure is followed with the REF, OSS-P, and OSS models. At this level, it seems worth recalling that OSS-P refers to the optimized single-step model that has been introduced in reference [11] while OSS refers to the present modelling proposal. As expected, the three models lead to quite similar results and, for the sake of conciseness, only the flame kernel development obtained with the REF chemistry is illustrated in Fig. 18.

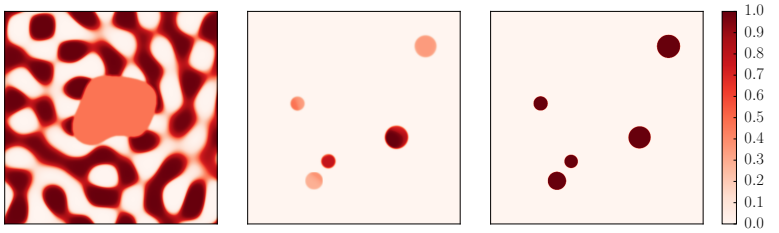

Fig. 19. Fields of the normalized pre-exponential factors (K_{P} and K_{I}) and weighting function K^* at $t^* = 0.0$ (i.e., $t^+ = t_f^+ = 1.8$). Left: K_{P}, middle: K_{I}, and right: K^*.

In a second step of this computation, several hot spots are initialized in the fresh reactants at time $t^* = (t - t_f^+ \cdot \tau_L^0)/\tau_{i,0}^{mr} = 0.0$, which corresponds

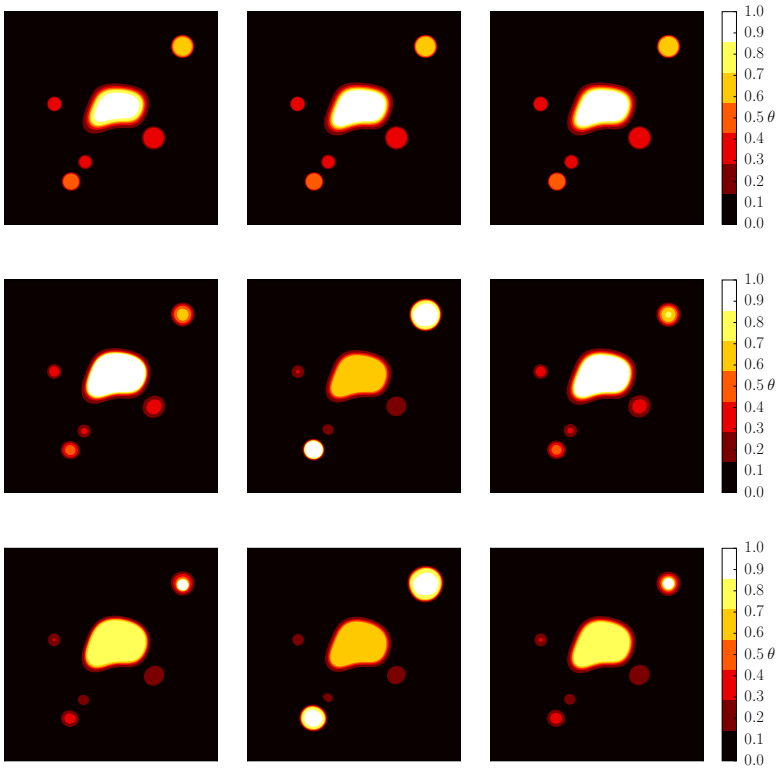

Fig. 20. Flame kernel growth and ignition of hot temperature spots: comparison, at three successive time-steps, between the normalized temperature fields obtained with the REF chemistry (left), OSS-P model (middle), and OSS model (right). Top: $t^* = 0.0$, middle: $t^* = 0.6$, and bottom: $t^* = 1.2$.

to $t^+ = t_f^+ = 1.8$. In the expression of t^* the quantity $\tau_{i,0}^{mr}$ stands for the reference ignition delay of the most reactive mixture fraction, as deduced from preliminary computations of homogeneous reactors performed for various equivalence ratio Φ and initial temperature T_u. Thus, an important difference with the previous set of computations lies in the unburnt gases temperature field, which is no longer homogeneous. The local temperature in the fresh reactants T_u has been settled so as to feature variations that range between 700 K and 1700 K, and thus it significantly exceeds the cross-over value at some locations. This leads to significant local variations of K_I that are depicted together with the variations of K^* in Fig. 19. As a consequence, both "ignition" and "propagation" modes are triggered.
From this new set of initial conditions, the simulation is run between $t^* = 0.0$

and $t^* = t_f^* = 1.2$. As expected, self-ignition processes take place while the flame kernel proceeds. Figure 20 reports a comparison between the normalized temperature fields $\theta(\boldsymbol{x}, t)$ obtained with the REF chemistry, OSS-P, and OSS model. The temperature fields issued from the REF chemistry and OSS model exhibit really close characteristics. Ignition processes start in a temperature spot located on the top right hand corner of the computational domain. It is quite remarkable that, using the OSS model, not only the ignition location but also the ignition dynamics are satisfactorily recovered. The quality of the agreement obtained between REF and OSS contrasts with the results issued from the OSS-P model. Indeed, within the OSS-P framework, ignition time is clearly underestimated, temperature levels tend to be overestimated in the ignited region, and finally ignition is also taking place on the bottom left hand corner of the computational domain, a behaviour that disagrees with the detailed chemistry of reference. This last set of results definitely confirms the relevance of the OSS model for situations featuring both flame propagation and ignition as well as its superiority over the recently-proposed OSS-P modelling framework.

4. Conclusion

The recently proposed optimized single-step (OSS-P) model has been extended to represent auto-ignition phenomena (above the cross-over temperature) in turbulent non-homogeneous reactive mixtures. In single-step models, the auto-ignition delay depends on two key parameters only : the pre-exponential factor and activation energy of the single-step Arrhenius law. In a way similar to the previous model development made by Erraiy *et al.* [11], an optimization procedure to quantify these parameters has been carried out and applied to methane-air mixtures and to a reference fuel characterizing ignition, namely the n-heptane. Once the optimization procedure completed, OSS ignition (OSS-I) and OSS propagation (OSS-P) models can be lumped into a single OSS model through the consideration of the cross-over temperature. An original tabulation method based on power and hyperbolic functions is also presented to make the access to the tabulated data more efficient in terms of both data reading and memory usage. The resulting ignition model is validated through applications to complexity-increasing configurations. Auto-ignition in two-dimensional flow configurations are first analyzed in both laminar and turbulent conditions. Then, the model is applied to the description of flame kernel development in heterogeneous auto-ignitive conditions. It is concluded that, for moderate CPU costs, the new OSS formulation, as described in this work, leads

to satisfactory results, which are in good agreement with reference data. Finally, it should be emphasized that the last test case, i.e., the flame kernel development in a non-homogeneous mixture featuring large variations of composition and temperature beyond the cross-over, offers quite interesting perspectives for future works and detailed analyses devoted to flame propagation in auto-ignitive conditions.

5. Acknowledgments

This work was performed using HPC resources from GENCI (Grand Equipement National de Calcul Intensif)-[CINES/IDRIS] under Grant DARI A0052B07456. The authors would like to thank P. Boivin (M2P2, Aix-Marseille University) who stimulated them to study ignition phenomena within the framework of the OSS chemistry.

Appendix A: Optimization based on the normalized residence time

As emphasized in Section 2, the standard OSS model for ignition does not perfectly match the temporal evolution of temperature. As a matter of fact, for any given set of initial conditions (P, T, and Φ), the pre-exponential factor is fixed according to the results of the optimization procedure. Thus, the temperature evolution follows a classical single-step Arrhenius law, and hence, does not account for changes in the steepness of the evolution due to the production and consumption of intermediate radicals. A more complex algorithm can be used to take into account the dynamic of ignition. First, a reduced or normalized residence time $t^* = t/\tau_i$ is introduced in such a manner that the whole evolution of the temperature, up to ignition, is captured in the interval $[0, 1]$ of the reduced time. Then, N_t discretization points (t_n^*) are chosen such that $t_n^* \in]0, 1]$ for $n \in \{1, N_t\}$. The cost function can be recast as a function of the temperature value reached at each intermediate point of the evolution

$$\mathrm{CF}(\boldsymbol{K_n}) = \|T_{\mathrm{OSS}}(t_n^*, \boldsymbol{K_n}) - T_{ref}(t_n^*)\| \quad \text{for} \quad n \in \{1, N_t\} \tag{31}$$

This new procedure generates N_t values of the pre-exponential factor for each initial condition, which results in an additional temporal dependency, and hence, a new dimension in the resulting table. By using the reduced time, the values obtained at the points (t_n^*) are identical for each set of initial conditions, thus avoiding the need to tabulate (t_n^*): only the ignition delay τ_i

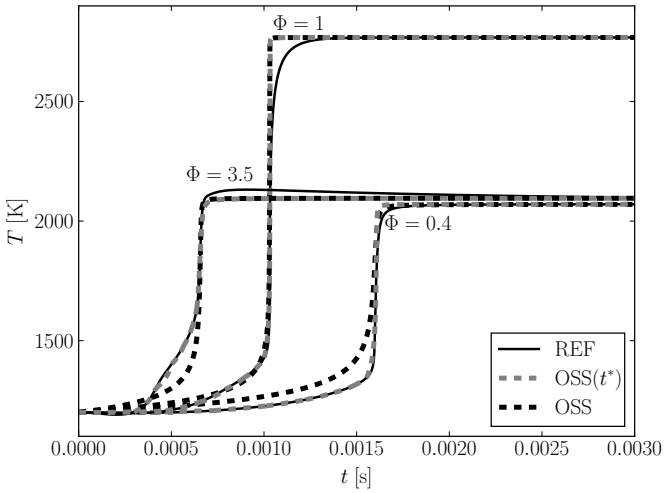

Fig. 21. Comparison between temperature evolutions obtained with the REF chemistry and using either the ignition OSS or the normalized residence time OSS(t^*) optimized chemistry for three distinct n-heptane/air mixtures.

is stored in the table. Considering that the steepness of the evolution of the temperature increases while approaching the ignition delay, it is necessary to locate a sufficiently large number of points while approaching $t^* = 1$. To this purpose, a temporal refinement function f_t is introduced in a way similar to the one retained for the discretization of the mixture fraction. However, f_t is a one-sided refined function meaning that the refinement takes solely place in the vicinity of t^* equals to unity. Starting from a linear discretization with N_t points in the interval $]0, 1]$, the function f_t generates values of t_n^* in such a manner that the density of the discretization (i.e., the number of points per unit t^*) increases as the value $t^* = 1$ is approached. The expression of f_t reads as

$$f_t(t^*) = \beta \frac{\alpha^{t^*} - 1}{\alpha^{t^*} + 1} \quad \text{where} \quad \alpha = \frac{\beta + 1}{\beta - 1} \tag{32}$$

In this expression, the parameter $\beta \in]1, 2[$ is the stretching parameter which determines the concentration of points around $t^* = 1$. Figure 21 compares the results obtained with both the ignition delay-optimized OSS chemistry and the reference chemistry for a n-heptane/air mixture initially at 1200 K and 5 bar. It can be seen that not only the ignition delay is also correctly restored, but the whole evolution of the temperature is perfectly

reproduced until ignition occurs with the reduced time-optimized procedure.

However, in practice, this new procedure may reveal itself quite computational demanding for more relevant applications to non-homogeneous mixtures. As a matter of fact, by adding a new dimension to the tabulation ($N_t + 1$ points for each initial condition), the size of the table may indeed significantly increase. Furthermore, it should be recalled that the purpose of the OSS model is to provide a cost-efficient method for solving chemistry in complex turbulent reactive flow fields. In such configurations, the variables of interest might be either averaged or filtered values. When considering for example the reduced time and the composition (e.g., the mixture fraction ξ), the unresolved covariance between both variables has yet to be determined, which rises some additional modelling issues. Addressing such difficulties is outside the scope of the OSS model, which aims at remaining as simple and as less computational-demanding as possible.

Appendix B: Evaluation of the cross-over temperature

Several expressions have been proposed for the cross-over temperature in the literature, see for instance references [25, 33, 38, 39]. In two of the aforementioned references [38, 39], the cross-over temperature corresponds to the temperature reached in the inner layer of a premixed flame. It can be interpreted as the temperature at which termination reactions prevail against the chain-branching reactions [40, 41]. The expression of the cross-over temperature T_c can be also deduced from the H_2/O_2 sub-mechanism, which can be considered as the kernel of any hydrocarbon chemistry [25, 33].

Table 1: Simplified ignition chemistry of H_2/O_2 [25].

	Reaction
(1f)	$H + O_2 \rightarrow OH + O$
(2f)	$H_2 + O \rightarrow OH + H$
(3f)	$H_2 + OH \rightarrow H_2O + H$
(4f)	$H + O_2 + M \rightarrow HO_2 + M$
(6b)	$H_2 + O_2 \rightarrow HO_2 + H$
(10f)	$H_2O_2 + M \rightarrow OH + OH + M$
(11f)	$HO_2 + HO_2 \rightarrow H_2O_2 + O_2$
(12f)	$HO_2 + H_2 \rightarrow H_2O_2 + H$

Prior to ignition, H_2/O_2 chemistry can be studied using the simplified system given in Table 1. Above the cross-over temperature, the evaluation

of which will be discussed below, chain-branching explosion takes place. It is dominated by reactions (1f), (2f), (3f), (4f), and (6b). Below the cross-over temperature, the recombination step (4f) prevails against the shuffle reactions (1f), (2f), (3f) and maintains the H radical concentration at very low values, there is no chain-branching and ignition proceeds instead through an alternative path involving HO_2 and H_2O_2, with production and consumption rates controlled by chemical reactions (10f), (11f), and (12f).

Ignition below the cross-over

In this case, according to Sanchez and Williams [25], the ignition can be described on the basis of reactions (3f), (4f), (10f), (11f), and (12f). Thus, the radical pool corresponds to four chemical species: H, OH, HO_2, and H_2O_2. Its evolution is governed by the following set of equations[2]

$$\frac{\mathrm{d}C_{\mathrm{H}}}{\mathrm{d}t} = k_{3\mathrm{f}}\, C_{\mathrm{OH}} C_{\mathrm{H_2}} - k_{4\mathrm{f}}\, C_{\mathrm{H}} C_{\mathrm{O_2}} C_{\mathrm{M4}} + k_{12\mathrm{f}}\, C_{\mathrm{HO_2}} C_{\mathrm{H_2}} \tag{33}$$

$$\frac{\mathrm{d}C_{\mathrm{OH}}}{\mathrm{d}t} = -k_{3\mathrm{f}}\, C_{\mathrm{OH}} C_{\mathrm{H_2}} + 2\, k_{10\mathrm{f}}\, C_{\mathrm{H_2O_2}} C_{\mathrm{M10}} \tag{34}$$

$$\frac{\mathrm{d}C_{\mathrm{HO_2}}}{\mathrm{d}t} = k_{4\mathrm{f}}\, C_{\mathrm{H}} C_{\mathrm{O_2}} C_{\mathrm{M4}} - 2\, k_{11\mathrm{f}}\, C_{\mathrm{HO_2}} C_{\mathrm{HO_2}} - k_{12\mathrm{f}}\, C_{\mathrm{HO_2}} C_{\mathrm{H_2}} \tag{35}$$

$$\frac{\mathrm{d}C_{\mathrm{H_2O_2}}}{\mathrm{d}t} = -k_{10\mathrm{f}}\, C_{\mathrm{H_2O_2}} C_{\mathrm{M10}} + 2\, k_{11\mathrm{f}}\, C_{\mathrm{HO_2}} C_{\mathrm{HO_2}} + k_{12\mathrm{f}}\, C_{\mathrm{HO_2}} C_{\mathrm{H_2}} \tag{36}$$

which can be linearly combined to eliminate reactions (3f), (4f), and (11f), thus leading to an evolution equation of the radical pool concentration ($C_{\mathrm{H}} + C_{\mathrm{OH}} + C_{\mathrm{HO_2}} + C_{\mathrm{H_2O_2}}$)

$$\frac{\mathrm{d}}{\mathrm{d}t}\left(C_{\mathrm{H}} + C_{\mathrm{OH}} + C_{\mathrm{HO_2}} + C_{\mathrm{H_2O_2}}\right) = k_{12\mathrm{f}}\, C_{\mathrm{HO_2}} C_{\mathrm{H_2}} - k_{10\mathrm{f}}\, C_{\mathrm{H_2O_2}} C_{\mathrm{M10}} \tag{37}$$

The application of the QSS assumption on H and OH allows to obtain

$$k_{4\mathrm{f}}\, C_{\mathrm{H}} C_{\mathrm{O_2}} C_{\mathrm{M4}} = k_{12\mathrm{f}}\, C_{\mathrm{HO_2}} C_{\mathrm{H_2}} + 2\, k_{10\mathrm{f}}\, C_{\mathrm{H_2O_2}} C_{\mathrm{M10}} \tag{38}$$

which together with the QSSA of the hydroperoxyl radical $C_{\mathrm{HO_2}}$, gives

$$k_{11\mathrm{f}}\, C_{\mathrm{HO_2}} C_{\mathrm{HO_2}} = k_{10\mathrm{f}}\, C_{\mathrm{H_2O_2}} C_{\mathrm{M10}} \tag{39}$$

This allows to relate the concentration in hydroperoxyl radical $C_{\mathrm{HO_2}}$ to $C_{\mathrm{H_2O_2}}$ and C_{M10}

$$C_{\mathrm{HO_2}} = \left(\frac{k_{10\mathrm{f}}}{k_{11\mathrm{f}}}\right)^{1/2} C_{\mathrm{H_2O_2}}^{1/2} C_{\mathrm{M10}}^{1/2} \tag{40}$$

[2]The quantities C_{M4} and C_{M10} denote species concentrations weighted by the third-body (i.e., Chaperon) efficiencies

which shows that the elementary step (12f) is autocatalytic in the sense that it produces H_2O_2 with a rate that is proportional to the square root of its concentration. Ignition below crossover takes place as a thermal explosion [25] with the temperature evolution driven by (10f) and hydrogen peroxide production driven by (12f).

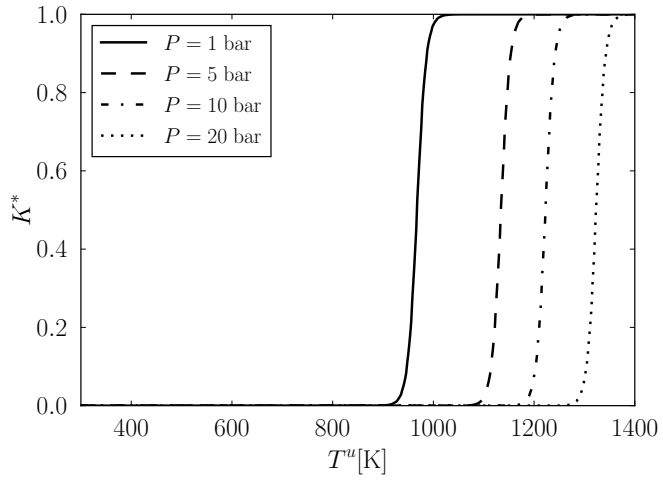

Fig. 22. Evolutions, at various pressure levels, of the weighting function K^* for a stoichiometric mixture of methane-oxygen, over the range of temperature considered in Fig 3.

Ignition above the cross-over

The temporal evolution of the radical pool is reduced to the following system of equations

$$\begin{aligned}\frac{\mathrm{d}C_{\mathrm{H}}}{\mathrm{d}t} &= -k_{1\mathrm{f}}\,C_{\mathrm{O}_2}C_{\mathrm{H}} + k_{2\mathrm{f}}\,C_{\mathrm{H}_2}C_{\mathrm{O}} + k_{3\mathrm{f}}\,C_{\mathrm{H}_2}C_{\mathrm{OH}} - k_{4\mathrm{f}}\,C_{\mathrm{M4}}C_{\mathrm{O}_2}C_{\mathrm{H}} \\ &+ k_{6\mathrm{b}}\,C_{\mathrm{O}_2}C_{\mathrm{H}_2} \qquad (41)\\ \frac{\mathrm{d}C_{\mathrm{O}}}{\mathrm{d}t} &= k_{1\mathrm{f}}\,C_{\mathrm{O}_2}C_{\mathrm{H}} - k_{2\mathrm{f}}\,C_{\mathrm{H}_2}C_{\mathrm{O}} \qquad (42)\\ \frac{\mathrm{d}C_{\mathrm{OH}}}{\mathrm{d}t} &= k_{1\mathrm{f}}\,C_{\mathrm{O}_2}C_{\mathrm{H}} + k_{2\mathrm{f}}\,C_{\mathrm{H}_2}C_{\mathrm{O}} - k_{3\mathrm{f}}\,C_{\mathrm{H}_2}C_{\mathrm{OH}} \qquad (43)\end{aligned}$$

which, as previously shown in reference [25], can be linearly combined to eliminate fast reactions (2f) and (3f), thus yielding to

$$\frac{\mathrm{d}}{\mathrm{d}t}\left(C_{\mathrm{H}} + 2C_{\mathrm{O}} + C_{\mathrm{OH}}\right) = \left(2k_{1\mathrm{f}} - k_{4\mathrm{f}}\,C_{\mathrm{M4}}\right)C_{\mathrm{O}_2}C_{\mathrm{H}} + k_{6\mathrm{b}}\,C_{\mathrm{O}_2}C_{\mathrm{H}_2} \qquad (44)$$

This equation indicates that an exponential growth of the radical pool concentration takes place only if $2k_{1\mathrm{f}} > k_{4\mathrm{f}}\, C_{\mathrm{M4}}$, which leads to the definition of a cross-over temperature T_c by the equation

$$2k_{1\mathrm{f}} = k_{4\mathrm{f}}\, C_{\mathrm{M4}} \tag{45}$$

The value of T_c depends on the composition and pressure through the third-body (i.e., Chaperon) efficiencies. This dependency is illustrated in Fig. 22, which reports the weighing function $(K_{\mathrm{PI}} - K_{\mathrm{P}})/(K_{\mathrm{I}} - K_{\mathrm{P}})$ plotted versus the fresh mixture temperature T^u. This figure does show that there is a significant influence of the operative pressure.

References

[1] R. W. Bilger, S. B. Pope, K. N. C. Bray, J. F. Driscoll, Paradigms in turbulent combustion research 30 (2005) 21–42.

[2] C. K. Westbrook, W. J. Pitz, O. Herbinet, H. J. Curran, E. J. Silke, A comprehensive detailed chemical kinetic reaction mechanism for combustion of n-alkane hydrocarbons from n-octane to n-hexadecane, Combustion and Flame 156 (1) (2009) 181–199.

[3] M. Mehl, W. J. Pitz, C. K. Westbrook, H. J. Curran, Kinetic modeling of gasoline surrogate components and mixtures under engine conditions, Proceedings of the Combustion Institute 33 (1) (2011) 193–200.

[4] T. Kreutz, C. Law, Ignition in nonpremixed counterflowing hydrogen versus heated air: Computational study with skeletal and reduced chemistry, Combustion and Flame 114 (3) (1998) 436–456.

[5] P. Lindstedt, Modeling of the chemical complexities of flames, Symposium (International) on Combustion 27 (1) (1998) 269–285.

[6] E. Fernández-Tarrazo, A. L. Sánchez, A. Liñán, F. A. Williams, A simple one-step chemistry model for partially premixed hydrocarbon combustion, Combustion and Flame 147 (1) (2006) 32–38.

[7] T. Lu, C. K. Law, A criterion based on computational singular perturbation for the identification of quasi steady state species: A reduced mechanism for methane oxidation with NO chemistry, Combustion and Flame 154 (4) (2008) 761–774.

[8] P. Boivin, C. Jimenez, A. Sánchez, F. Williams, An explicit reduced mechanism for H2-air combustion, Proceedings of the Combustion Institute 33 (1) (2011) 517–523.

[9] P. Boivin, A. L. Sánchez, F. A. Williams, Explicit analytic prediction for hydrogen–oxygen ignition times at temperatures below crossover, Combustion and Flame 159 (2) (2012) 748–752.

[10] P. Boivin, A. L. Sánchez, F. A. Williams, Four-step and three-step systematically reduced chemistry for wide-range H2–air combustion problems, Combustion and Flame 160 (1) (2013) 76–82.

[11] A. Er-raiy, Z. Bouali, J. Réveillon, A. Mura, Optimized single-step (OSS) chemistry models for the simulation of turbulent premixed flame propagation, Combustion and Flame 192 (2018) 130–148.

[12] J. W. Dold, Premixed flames modelled with thermally sensitive intermediate branching kinetics, Combustion Theory and Modelling 11 (6) (2007) 909–948.

[13] B. Franzelli, E. Riber, M. Sanjosé, T. Poinsot, A two-step chemical scheme for kerosene–air premixed flames, Combustion and Flame 157 (7) (2010) 1364–1373.

[14] M. Cailler, N. Darabiha, D. Veynante, B. Fiorina, Building-up virtual optimized mechanism for flame modeling, Proceedings of the Combustion Institute 36 (1) (2017) 1251–1258.

[15] A. Misdariis, O. Vermorel, T. Poinsot, A methodology based on reduced schemes to compute autoignition and propagation in internal combustion engines, Proceedings of the Combustion Institute 35 (3) (2015) 3001–3008.

[16] S. Gordon, B. J. McBride, Computer program for calculation of complex chemical equilibrium compositions, rocket performance, incident and reflected shocks, and Chapman – Jouguet detonations, Tech. Rep. NASA-SP-273, NASA Lewis Research Center (1976).

[17] D. G. Goodwin, H. K. Moffat, R. L. Speth, Cantera: An object-oriented software toolkit for chemical kinetics, thermodynamics, and transport processes, http://www.cantera.org, version 2.3.0 (2017).

[18] F. A. Williams, Combustion Theory, CRC Press, 1985.

[19] R. P. Brent, Algorithms for minimization without derivatives, Englewood Cliffs, N.J. : Prentice-Hall, 1973.

[20] F. Battin-Leclerc, Detailed chemical kinetic models for the low-temperature combustion of hydrocarbons with application to gasoline and diesel fuel surrogates, Progress in Energy and Combustion Science 34 (4) (2008) 440–498.

[21] Z. Bouali, C. Pera, J. Reveillon, Numerical analysis of the influence of two-phase flow mass and heat transfer on n-heptane autoignition, Combustion and Flame 159 (6) (2012) 2056–2068.

[22] A. Patel, S.-C. Kong, R. D. Reitz, Development and validation of a reduced reaction mechanism for HCCI engine simulations, in: SAE Technical Paper, SAE International, 2004.

[23] C. Westbrook, F. Dryer, Chemical kinetic modeling of hydrocarbon combustion, Progress in Energy and Combustion Science 10 (1) (1984) 1–57.

[24] G. von Elbe, B. Lewis, Mechanism of the thermal reaction between hydrogen and oxygen, The Journal of Chemical Physics 10 (6) (1942) 366–393.

[25] A. L. Sánchez, F. A. Williams, Recent advances in understanding of flammability characteristics of hydrogen, Progress in Energy and Combustion Science 41 (2014) 1–55.

[26] T. Lu, C. K. Law, A directed relation graph method for mechanism reduction, Proceedings of the Combustion Institute 30 (2005) 1333–1341.

[27] T. Jaravel, E. Riber, B. Cuenot, P. Pepiot, Prediction of flame structure and pollutant formation of Sandia flame D using large eddy simulation with direct integration of chemical kinetics, Combustion and Flame 188 (2018) 180 – 198.

[28] G. P. Smith, D. M. Golden, M. Frenklach, N. W. Moriarty, B. Eiteneer, M. Goldenberg, C. T. Bowman, R. K. Hanson, S. Song, W. C. Gardiner, V. V. Lissianski, Z. Qin, Gri-mech 3.0 (1999).
URL http://www.me.berkeley.edu/gri-mech/

[29] J. Reveillon, C. Pera, Z. Bouali, Examples of the potential of DNS for the understanding of reactive multiphase flows, International Journal of Spray and Combustion Dynamics 3 (1) (2011) 63–92.

[30] R. D. Falgout, U. M. Yang, HYPRE: A library of high performance preconditioners, in: International Conference on Computational Science, Springer, 2002, pp. 632–641.

[31] S. Zhao, A. Er-raiy, Z. Bouali, A. Mura, Dynamics and kinematics of the reactive scalar gradient in weakly turbulent premixed flames, Combustion and Flame 198 (2018) 436–454.

[32] A. C. Hindmarsh, P. N. Brown, K. E. Grant, S. L. Lee, R. Serban, D. E. Shumaker, C. S. Woodward, SUNDIALS: Suite of Nonlinear and Differential/Algebraic Equation Solvers, ACM Trans. Math. Softw. 31 (3) (2005) 363–396.

[33] C. K. Westbrook, Chemical kinetics of hydrocarbon ignition in practical combustion systems, Proceedings of the Combustion Institute 28 (2) (2000) 1563–1577.

[34] J. Reveillon, Numerical procedures to generate and to visualize flow fields from analytical or experimental statistics, Journal of Flow Visualization and Image Processing 12 (3) (2005) 251–269.

[35] S. Mukhopadhyay, J. Abraham, Influence of compositional stratification on autoignition in n-heptane/air mixtures, Combustion and Flame 158 (6) (2011) 1064 – 1075.

[36] R. S. Rogallo, Numerical experiments in homogeneous turbulence, Tech. Rep. NASA-TM-81315, NASA Ames Research Center (1981).

[37] T. Passot, A. Pouquet, Numerical simulation of compressible homogeneous flows in the turbulent regime, Journal of Fluid Mechanics 181 (1987) 441–466.

[38] N. Peters, F. Williams, The asymptotic structure of stoichiometric methane-air flames, Combustion and Flame 68 (2) (1987) 185–207.

[39] N. Peters, Turbulent Combustion, Cambridge Monographs on Mechanics, Cambridge University Press, 2000.

[40] N. Peters, Kinetic foundation of thermal flame theory, in: Advances in Combustion Science: In Honor of Ya. B. Zel'dovich, American Institute of Aeronautics and Astronautics, 1997, pp. 73–91.

[41] J. Buckmaster, P. Clavin, A. Liñán, M. Matalon, N. Peters, G. Sivashinsky, F. A. Williams, Combustion theory and modeling, Proceedings of the Combustion Institute 30 (1) (2005) 1–19.